Cislunar Maneuver Detection and Classification

Charles J. Wetterer[1], C. Channing Chow II[2], Jason, Baldwin[3], Micah Dilley[1], Keric Hill[1], Helen Montell-Weiland[1], Paul Billings[1], Christopher Craft[1], and James Frith[4]
[1]KBR, [2]Cloudstone Innovations, [3]Complex Futures, and
[4]Air Force Research Laboratory

ABSTRACT

Orbit determination and tracking of objects in cislunar space is more challenging in part because of the added complexity of the orbital dynamics due to the non-negligible influence of the Moon's gravity. Despite this, in a previous paper we showed that the Unscented Kalman Filter (UKF) successfully converged to a solution in most situations when using an appropriate dynamics model to propagate the state. Here, we employ a capability known as the Infinity Filter Framework (IFF) to build the estimation filter together with NASA's General Mission Analysis Tool (GMAT) as the dynamics model. The simulated orbital states used in the analysis are generated using a different, yet comparable, high-fidelity dynamics model. In this paper, we apply the UKF in an Interacting Multiple Model (IMM) approach to identify maneuvers in simulated data of a differentially corrected halo orbit using passive RF observations. Passive RF observations were chosen to allow consistent daily observations during the day or night and to legitimize the assumption that the observations can be associated with the object despite the maneuver. We investigate maneuvers from the L1 periodic Halo family (i.e., H1) with a range of delta-V magnitudes (9 values between 0.1 m/s and 298.1 m/s) and directions (radial, in-track and cross-track), enabling the exploration of both extremes of maneuver detection. For small velocities, the maneuver may be too small to trigger detection while for large velocities, the filter may diverge due to the larger uncertainties and non-linear dynamics. Observations are time difference of arrival (TDOA) and frequency difference of arrival (FDOA) values from a 3-site hypothetical ground-based passive RF array. The three baselines yield 6 total measurements (3 TDOAs and 3 FDOAs) for each time step, chosen to be a 300 second cadence. With a single Earth-based passive RF array, there are daily data gaps or outages corresponding to when the object is below the local horizon of a sensor. To explore various detection possibilities, the maneuvers take place at four different epochs: (1) the beginning of daily observations, (2) midway through the daily observations, (3) at the start of the data gap between observations, and (4) midway through the data gap. Finally, the maneuver model in the IMM uses four different isotropic process noise values (0.1 to 100 m/s) to detect the presence of maneuvers and classify their magnitudes. For a selection of maneuvers, multiple maneuver models with direction-specific process noise values are employed to demonstrate directional classification of the maneuver as well. We show how the IMM filters behave when processing the different cislunar passive RF observation sets and the effectiveness and limits to cislunar maneuver detection and classification.

1. INTRODUCTION

Our previous papers provide an overview of the expected photometric and astrometric measurements of objects in cislunar orbits [1] and a demonstration of using these observations to track objects in these orbits using estimation filters [2]. In this paper, we explore the detection and characterization of impulsive maneuvers for an object in a cislunar orbit using similar estimation filters. Specifically, we employ the Interacting Multiple Model (IMM) [3] with a non-maneuver model (low process noise) and maneuver model(s) (higher process noise) tracking the object simultaneously. After a maneuver, the weight of the maneuver model (directly related to how well the model is predicting the state of the object) ideally becomes greater than the non-maneuver model, thus providing a means of maneuver detection. We will not only show maneuver detection using an IMM, but also maneuver characterization by employing multiple maneuver models (e.g., radial vs. in-track vs. cross-track delta-V's) and observing the associated weights of each through the maneuver.

The details of the maneuvers and subsequent generation of the observations are described in the next section. The Infinity Filter Framework (IFF) and NASA's General Mission Analysis Tool (GMAT) [4] are again used as the basis for the estimation filter, and the manner in which these capabilities create the IMM is described in the following

section. Finally, the results of the IMM are presented for both a maneuver detection (with a single maneuver model) and characterization (with multiple maneuver models).

2. ORBITS AND OBSERVATIONS

We chose a single cislunar halo orbit (H1 (100N)) from our previous paper [2] as the starting orbit. At 4 different starting epochs (6 hours apart) a near instantaneous thrust is applied with 3 different maneuver directions (radial, in-track, and cross-track) and 11 different maneuver delta-V magnitudes (0.1, 0.3, 0.7, 2.0, 5.5, 14.8, 40.3, 109.7, 298.1, 405.2, and 810.3 m/s) leading to 132 different maneuver orbits. As in our previous papers, the propagator that generates the orbits uses a realistic inertial model including third-body effects from the Moon and Sun. The orbits are differentially corrected to maintain the specific cislunar halo orbit up to the point of the maneuver, and then allowed to fly ballistically for approximately four days after the maneuver. All orbits start at 2019-07-19T19:38:14.4 UTC. Figure 1 displays positional difference from the no-maneuver orbit for the different epoch 1 maneuvers (maneuver at 2019-07-23T10:51:15.8), which takes place just at the start of daily observations defined by visibility from a passive RF ground-based array. The other epochs are mid observations (epoch 2 – maneuver at 2019-07-23T16:51:15.8), start of gap (epoch 3 – maneuver at 2019-07-23T22:51:15.8) and mid gap (epoch 4 – maneuver at 2019-07-24T04:51:15.8).

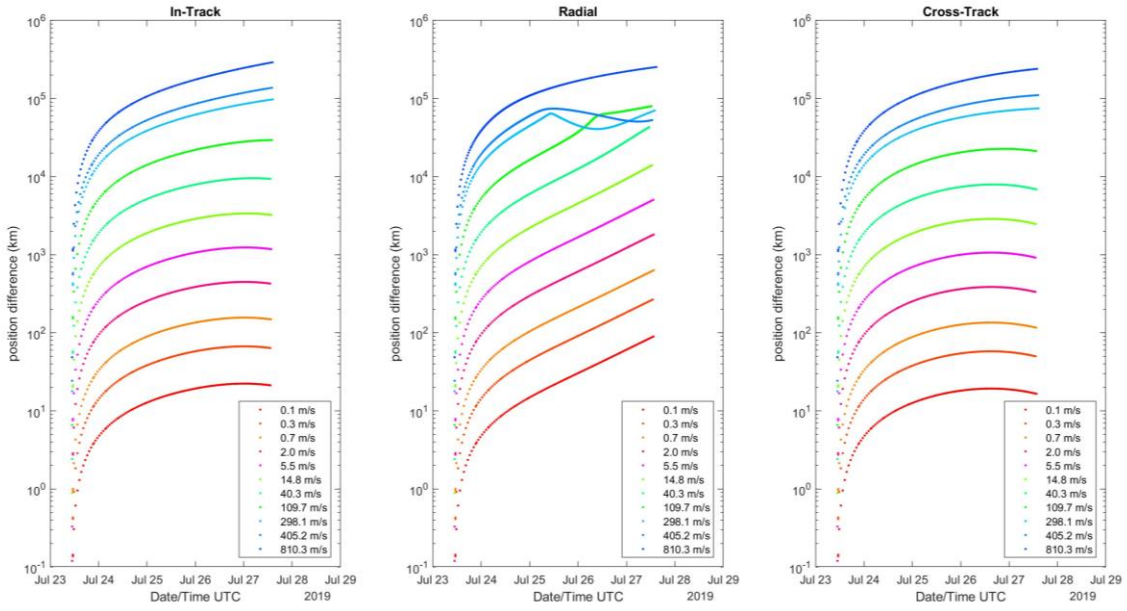

Figure 1. Positional differences as functions of time for epoch 1 maneuver orbits showing variations as functions of the impulsive maneuver delta-V magnitude.

Passive RF observations are simulated from a notional sensor array, with a 300 s cadence, with locations at Maui (20.7° N, 156.4° W) - Midway Island (28.2° N 177.4° W) - Palmyra Island (5.9° N 162.1° W). While any type of observation could be used, we choose passive RF to allow for consistent observations night and day and to demonstrate a different type of observation from those used in the previous papers. No exclusion zones for the Sun or Moon are employed, so daily observation gaps occur only when the object is below the local horizon for one or more of the sensors. Figure 2 shows the intervals of observations (black horizontal bars) and associated observation gaps for the four epochs with the vertical red lines indicating the time of the maneuver. The resulting measurements are the time difference of arrival (TDOA) and frequency difference of arrival (FDOA) values from each of the three different baselines per time step, thus yielding six measurements total per time step. TDOAs are measured in seconds and are the result of the different distances between the sensors and the object coupled with the finite speed of light. FDOAs are measured in Hertz and are the result of the different relative velocities between the sensors and the object. The frequency is set to the Ku band (12.5 GHz), and the simulated Gaussian uncertainty is set to 10^{-8} s for TDOA and 0.03 Hz for FDOA with no timing bias and an assumed known tropospheric delay.

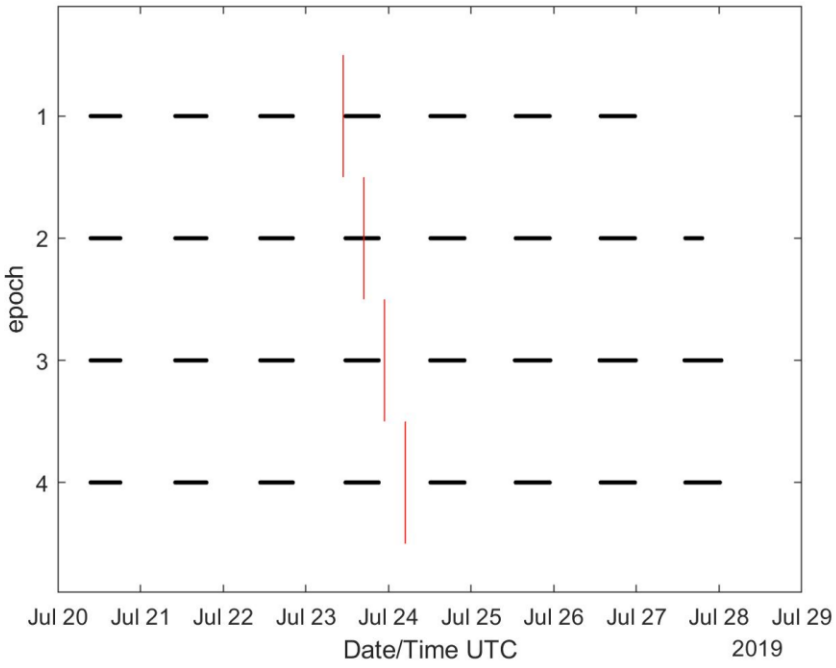

Figure 2. Observation periods (black horizontal lines) and maneuver times (red vertical lines) for each epoch to examine the impact of maneuver timing on detection/characterization.

3. INTERACTING MULTIPLE MODEL

The IFF, described in our previous paper [2], is a MATLAB-based software suite that encodes a generalized framework capable of constructing various types of filters from key components or modules. An IMM is an estimation filter with more than one dynamical model operating simultaneously where the states used by each model mixes at each time step according to the associated weights derived from how well the model predicts the current observations. In this paper, one model assumes no maneuvers and employs a very small process noise to account for any dynamical mismatch between the propagator used to generate the simulated data and the propagator used within the filter (e.g., GMAT). The other models have higher process noises to account for the possibility of a maneuver. The IFF is ideally suited for employing an IMM where the models are individual "particles" in the underlying IFF and the interacting occurs in the IFF's resampling step (Module-R). Three mixing probabilities and an initial weight for the maneuver particle(s) are required for the IMM. These are defined as $\rho_{NM} = 10^{-20}$ (probability of going from nominal to maneuver), $\rho_{MN} = 10^{-3}$ (probability of going from maneuver to nominal), $\rho_{MM} = 10^{-20}$ (probability of going from maneuver to maneuver if multiple maneuver particles are used), and $w_{init} = 10^{-5}$ (initial weight of maneuver model).

In the first analysis, an IMM with two particles (models) is employed. The first particle is an Unscented Kalman Filter (UKF) with an isotropic process noise (in acceleration) of 10^{-10} km/s^2. This is the so-called no-maneuver or nominal model. The second particle is a UKF with an isotropic process noise (in velocity) of either 0.1 m/s, 1 m/s, 10 m/s, or 100 m/s, which leads to 528 total processing cases (four epochs × eleven delta-V magnitudes × three delta-V directions × four process noises). A process noise of 1000 m/s is also investigated. This setting resulted in all runs exhibiting instances where a sigma point passed too close to the Moon's center, causing the estimated state to become unrealistic. With two particles, the transition probability matrix is given by

$$T = \begin{bmatrix} 1-\rho_{NM} & \rho_{MN} \\ \rho_{NM} & 1-\rho_{MN} \end{bmatrix} \quad (1)$$

In the second analysis, an IMM with four particles is employed. Again, the first (non-maneuver) particle is a UKF with an isotropic process noise (in acceleration) of 10^{-10} km/s^2. The maneuver particles are directional with a process noise in radial (particle 2), in-track (particle 3) and cross-track (particle 4) directions. Note that the radial/in-track/cross-track directions are defined with respect to the Earth. We analyze select maneuver orbits for all epochs and maneuver directions using particular process noise values, as detailed in Table 1. We discovered that radial maneuver particles with too small a process noise produce significant false maneuver detections, and so a lower limit of 10 m/s for the radial particle process noise is adopted. With four particles, the transition probability matrix is given by

$$T = \begin{bmatrix} 1-3\rho_{NM} & \rho_{MN} & \rho_{MN} & \rho_{MN} \\ \rho_{NM} & 1-\rho_{MN}-2\rho_{MM} & \rho_{MM} & \rho_{MM} \\ \rho_{NM} & \rho_{MM} & 1-\rho_{MN}-2\rho_{MM} & \rho_{MM} \\ \rho_{NM} & \rho_{MM} & \rho_{MM} & 1-\rho_{MN}-2\rho_{MM} \end{bmatrix} \quad (2)$$

Table 1. Directional IMM cases.

Delta-V (all epochs) (km/s)	Particle 2 (radial) process noise	Particle 3 (in-track) process noise	Particle 4 (cross-track) process noise
0.1, 0.3, 0.7, 2.0	10 m/s	0.1 m/s	0.1 m/s
2.0, 5.5, 14.8, 40.3	10 m/s	1 m/s	1 m/s
40.3, 109.7, 298.1, 405.2	100 m/s	100 m/s	100 m/s

4. ANALYSIS

4.1 Isotropic IMM

Table 2 displays the results for all 528 runs in the first analysis. A detection is defined as when the weight of the maneuver particle (particle 2) becomes greater than 0.5. The filter "recovers" from the detection when the overall positional error reduces to less than its pre-maneuver accuracy or 20 km, whichever is greater, and the maneuver particle's weight stays below 0.5. Within each cell are four symbols corresponding to the 0.1, 1, 10, and 100 m/s particle 2 isotropic process noise. Detections are denoted with a *, +, or | depending on whether the recovery is less than 2 days, greater than 2 days, or not within the set of observations (~4 days) respectively. Non-detections are denoted with a –, ~, or numerical value depending on whether the filter maintains track, loses track, or the maneuver particle's weight increases, but not above the 0.5 threshold. For the numerical values, it is a number between 1 and 9 corresponding to 10% to 90% as measured from the baseline pre-maneuver weight to one on a log scale. Only increases in the maneuver particle weight within a day after the maneuver are considered. In some high delta-V cases, problematic maneuver states are generated due to passing too close to the center of the Moon leading eventually to non-positive definite state covariances being generated when the maneuver particle mixes with the non-maneuver particle. When this occurs, the mixing is not done, and the maneuver particle's state and covariance are reset to allow the filter to proceed. These instances, however, are highlighted as a red symbol in the table. Finally, for each set of four maneuver particle process noise values for a particular orbit and epoch, the instance where the filter recovers fastest is highlighted in green.

From the low magnitude delta-V case results, it is evident that the IMM has a detection limit for small maneuvers. Generally, the detection limit is lowest for cross-track and highest for radial maneuvers. Figure 3 illustrates this by plotting the fraction detected as a function of maneuver velocity. A near 100% maneuver detection rate occurs for maneuver magnitudes greater than 1 m/s. Looking at the best recovery (green highlighted cases in Table 2) as a function of delta-V magnitude, generally as the magnitude of maneuver becomes larger, the larger maneuver particle process noise IMM instantiations yield better results. Figure 4 illustrates this by plotting the fraction a particular process noise has the best recovery after the maneuver (for the twelve different direction/epoch combinations for a particular delta-V magnitude) as a function of the delta-V magnitude. The trend is most evident when comparing the 0.1 m/s process noise (which performs best for lower delta-V magnitudes) to the 100 m/s process noise (which

performs best for higher delta-V magnitudes). Finally, it appears that the IMM has no upper limit for detection but can lose tracking if the maneuver is too large. Note that it is possible that some of these object orbits would "recover" if observations continued, but in several cases the filter has simply lost tracking. The slight dip in detection rate at high delta-V magnitudes in Figure 3 are those instances where the filter loses track of the object at the maneuver and yet the maneuver particle's weight never exceeded 0.5, although it could be argued that the simple fact that the filter lost track of the object is an indication that a maneuver took place. Instances of non-positive definite covariances in Module R become a problem only for the highest maneuvers (298.1 m/s and above). Figure 5 through Figure 10 show a sample position error as a function of time plot and particle weight as function of time plot (in log scale) for each of the symbols represented in Table 2.

Table 2. Isotropic IMM results.

Δv (m/s)	**radial**				**in-track**				**cross-track**			
Epoch	1	2	3	4	1	2	3	4	1	2	3	4
0.1	32--	----	----	----	*+21	**--	**--	+21-	**+-	****	****	***7
0.3	**1-	----	**--	**--	+**+	****	****	***9	**+*	****	****	****
0.7	+***	****	****	****	****	****	****	***+	**+*	****	****	**+*
2.0	+***	****	****	**++	**++	****	***+	***+	**+*	****	***+	****
5.5	*+**	+***	+*++	+*++	****	****	***+	**+*	**++	****	***+	*+**
14.8	+***	****	+*++	+*++	++**	****	+***	****	+++*	****	****	++**
40.3	++**	++**	+*+*	+*+*	+++*	****	+***	+++*	+++*	****	*+**	++**
109.7	+***	+***	+++*	|**+	||++	****	+*++	+++*	|++*	****	+++*	|+**
298.1	|***	++**	++**	++**	|+1+	*+++	||+*	||+|	++1+	***+	++**	+|||
405.2	||**	++**	||**	||**	|11|	*+++	|++*	+||+	+*++	+**+	|++*	||+~
810.3	+**	++**	|||*	||++	|5||	+++*	+++*	|||~	++*+	+*++	|||~	||+|

–	: no detection but maintains target
~	: no detection and filter loses target (diverges after maneuver)
1-9	: particle 2 weight at 10-90% in log scale at time of maneuver (as measured from baseline to 1)
|	: detection (particle 2 weight > 0.5), but filter loses target (diverges after maneuver)
+	: detection (particle 2 weight > 0.5), and filter takes > 2 days to recover
*	: detection (particle 2 weight > 0.5), and filter takes < 2 days to recover
(red)	: instance(s) of non-positive definite covariance in Module-R
(green)	: best detection of process noise group (shortest recovery) without instance of non-positive definite covariance

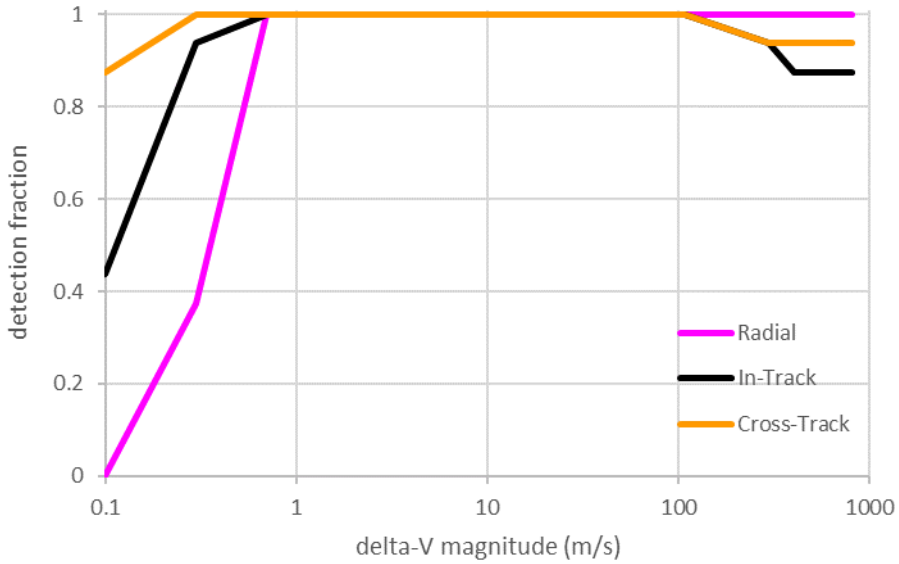

Figure 3. Fraction with correct maneuver detection as function of delta-V magnitude showing difference in low magnitude delta-V detection limit based on maneuver direction. Filter losing track of object accounts for lowering of high magnitude delta-V detection fraction.

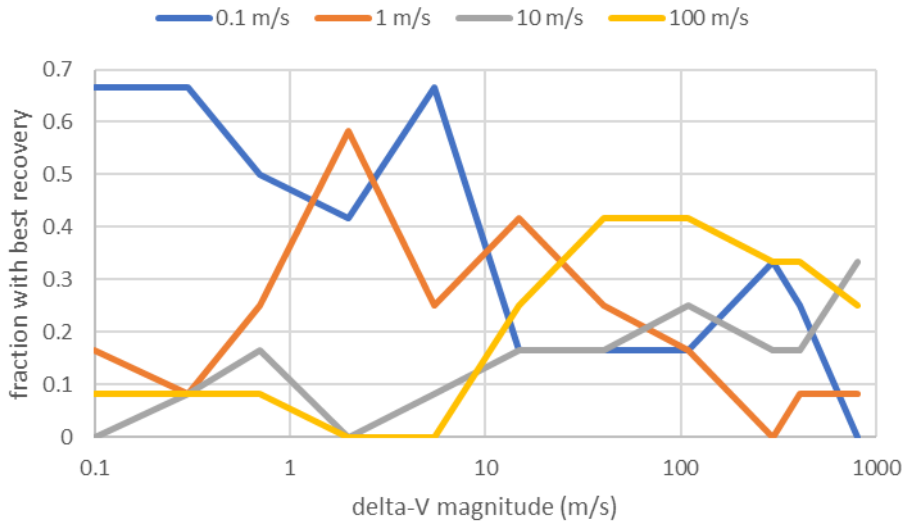

Figure 4. Fraction particular process noise has best recovery after maneuver (of the twelve different direction/epoch combinations per delta-V magnitude) versus delta-V magnitude showing better recovery of lower delta-V magnitude cases using lower process noise maneuver particles and better recovery of higher delta-V magnitude cases using higher process noise maneuver particles.

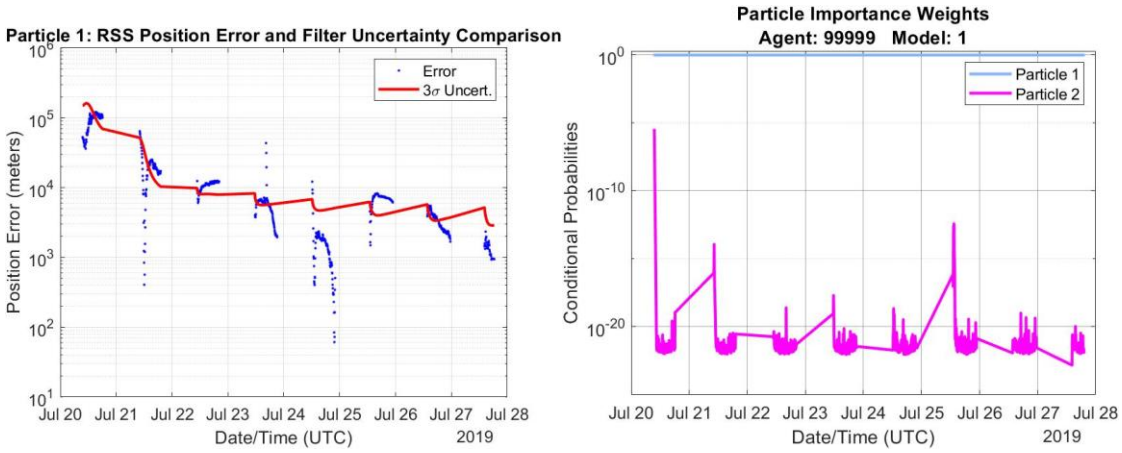

Figure 5. Example of no detection (- symbol in Table 2) since the weight (right) is well below 0.5 (epoch 2, 0.3 m/s radial maneuver, 1 m/s particle 2 (maneuver particle) process noise).

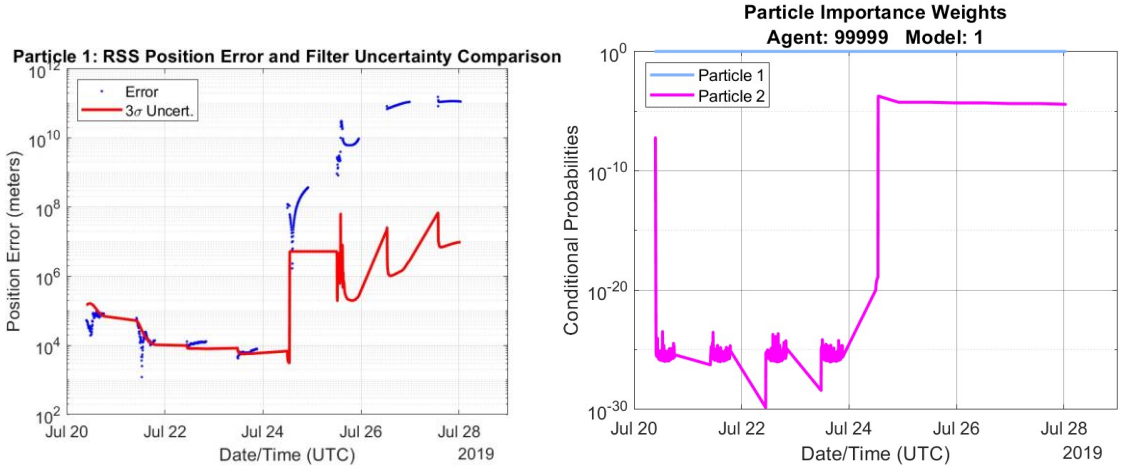

Figure 6. Example of no detection and loses track (~ symbol in Table 2) since errors (left) greatly exceed the estimated uncertainty region and the weight (right) is well below 0.5(epoch 3, 810.3 m/s cross-track maneuver, 100 m/s particle 2 (maneuver particle) process noise).

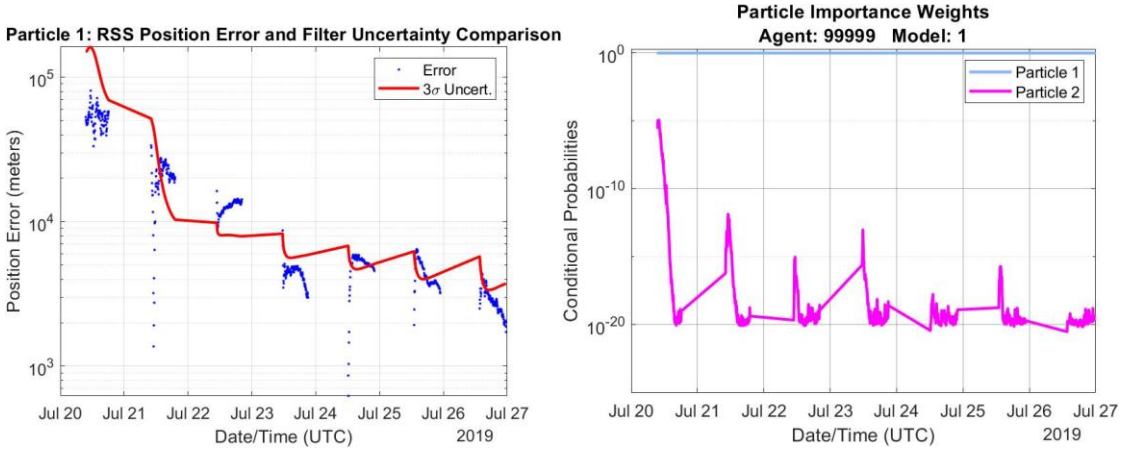

Figure 7. Example of particle 2 10-90% in log scale as measured from particle 1 baseline (# symbol in Table 2) (epoch 1, 0.1 m/s radial maneuver, 0.1 m/s particle 2 (maneuver particle) process noise).

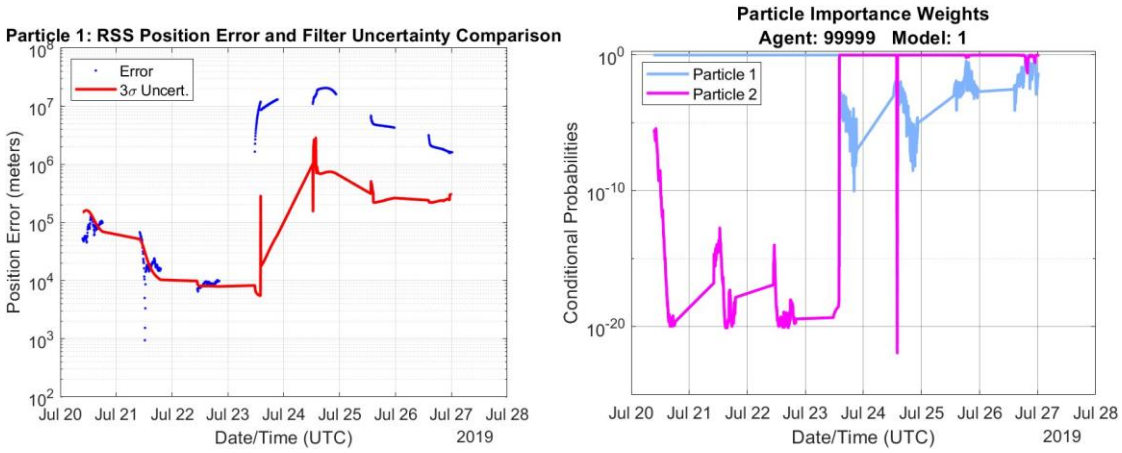

Figure 8. Example of detection but loses track (| symbol in Table 2) (epoch 1, 298.1 m/s in-track maneuver, 0.1 m/s particle 2 (maneuver particle) process noise).

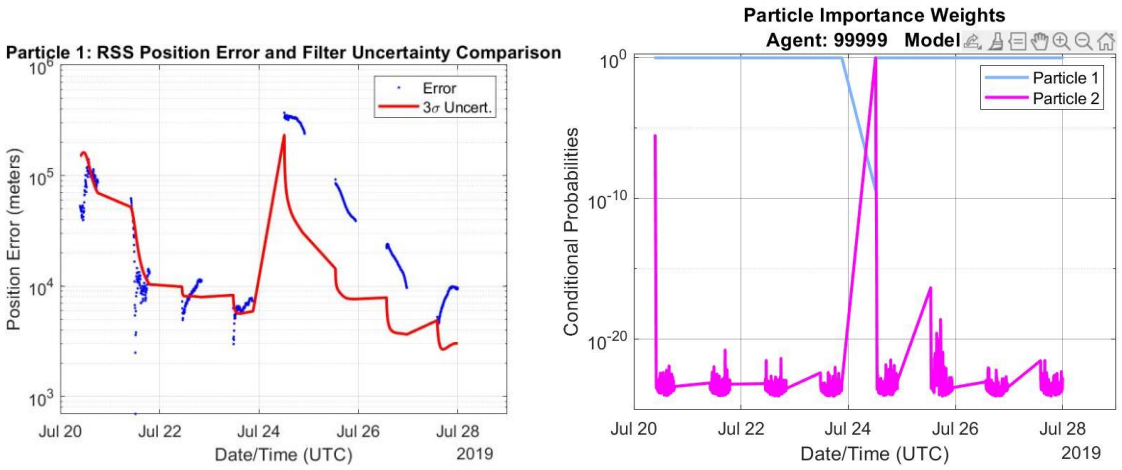

Figure 9. Example of detection but recovery after two days (+ symbol in Table 2) (epoch 3, 14.8 m/s radial maneuver, 10 m/s particle 2 (maneuver particle) process noise).

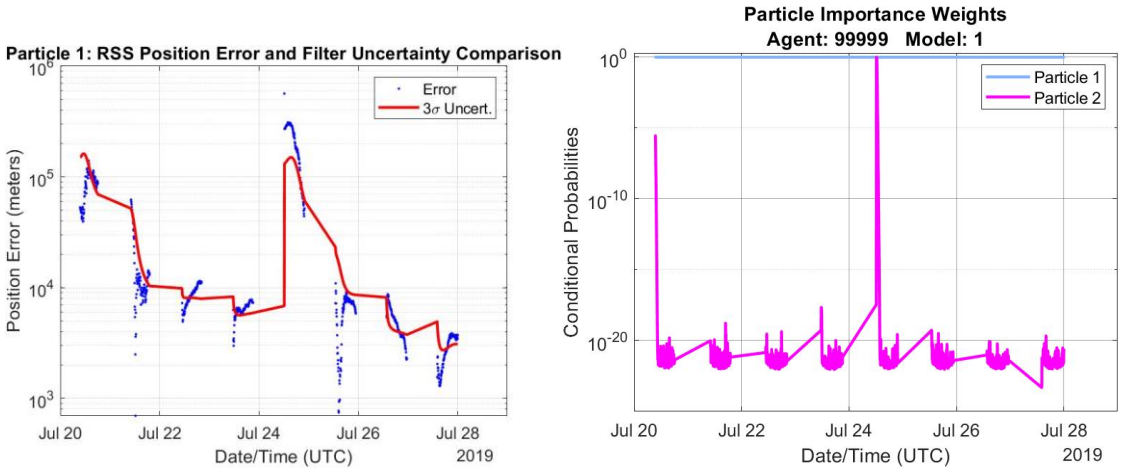

Figure 10. Example of detection and recovery before two days (symbol in Table 2) (epoch 3, 14.8 m/s radial maneuver, 1 m/s particle 2 (maneuver particle) process noise).*

4.2 Directional IMM

Table 3 displays the results for the three process noise distributions shown in Table 1. As in Table 2, *, +, or | denotes maneuver detections depending on whether the recovery is less than 2 days, greater than 2 days, or not within the set of observations respectively, and – or ~ denotes non-detections depending on whether the filter maintains track or not. A detection occurs when the sum of the weights of the three maneuver particles is greater than 0.5, and a recovery occurs when the total positional error is less than pre-maneuver value or 20 km, whichever is greater, and the sum of the weights of the three maneuver particles is less than 0.5. The second symbol for each case with a detection references the associated characterization direction: radial (R), in-track (I), cross-track (C), or multiple (X). A lower-case letter indicates that one or more additional false detections occurs after the initial detection and before filter recovery. Figure 11 and Figure 12 display sample results of the Directional IMM for a case of a maneuver detection and directional characterization and recovery within 2 days.

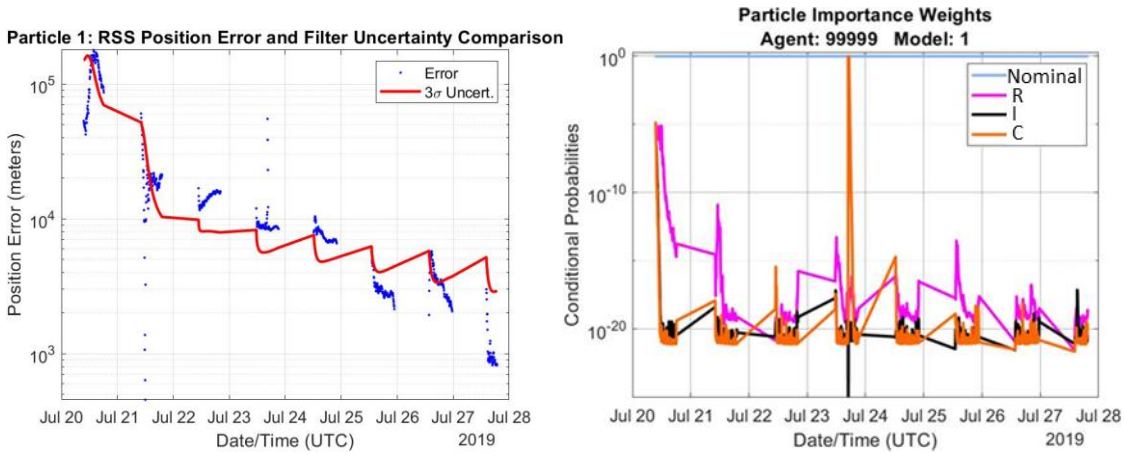

*Figure 11. Example of directional maneuver detection and recovery before two days (*C symbol in Table 3) (epoch 3, 2.0 m/s cross-track maneuver, 1 m/s particle 4 (cross-track maneuver particle) process noise).*

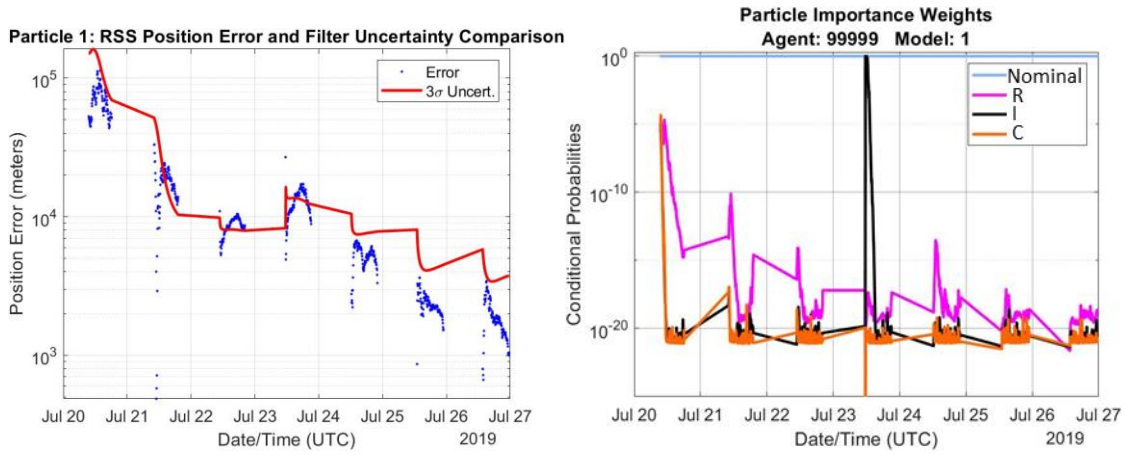

*Figure 12. Example of directional maneuver detection and recovery before two days (*I symbol in Table 3) (epoch 1, 5.5 m/s in-track maneuver, 1 m/s particle 3 (in-track maneuver particle) process noise).*

Table 3. Directional IMM results.

10 m/s radial, 0.1 m/s In-track and cross-track

Δv (m/s)	radial				in-track				cross-track			
Epoch	1	2	3	4	1	2	3	4	1	2	3	4
0.1	–	–	–	–	*I	*x	*x	*i	*r	*C	*c	*C
0.3	*x	*x	*X	*x	+r	*i	*X	*i	*C	*C	*C	*C
0.7	*x	*R	*R	*x	*i	*I	*R	*X	*C	*C	*c	*C
2.0	*i	*X	*r	*R	*r	*i	*r	*r	*C	*C	*c	*C

10 m/s radial, 1 m/s In-track and cross-track

Δv (m/s)	radial				in-track				cross-track			
Epoch	1	2	3	4	1	2	3	4	1	2	3	4
2.0	*r	*X	*r	*R	*R	*I	*r	*r	*C	*C	*C	*C
5.5	*r	*r	*R	*r	*I	*I	*r	*x	*C	*C	+c	+C
14.8	*r	*r	*r	*r	*I	*I	*r	*X	+c	*c	*X	+c
40.3	*r	*r	*R	+r	*i	*I	*x	+I	+X	*c	*c	*c

100 m/s radial, In-track and cross-track

Δv (m/s)	radial				in-track				cross-track			
Epoch	1	2	3	4	1	2	3	4	1	2	3	4
40.3	*r	*R	*r	*r	*i	*I	*i	*r	|c	*c	–	+c
109.7	+r	*R	+r	*x	+i	*I	*x	+i	*x	+c	*r	|r
298.1	*X	+r	*r	*x	*i	+i	*x	*i	*x	*i	|X	+x
405.2	*X	*r	*x	|x	+i	+i	*x	*x	+x	–	+x	|x

– : no detection but maintains target
~ : no detection and filter loses target (diverges after maneuver)
1–9 : particle 2-4 weight at 10-90% in log scale at time of maneuver
|X : detection (particles 2-4 sum weight > 0.5), but filter loses target
+X : detection (particles 2-4 sum weight > 0.5), takes >2-day recovery
*X : detection (particles 2-4 sum weight > 0.5), takes <2-day recovery
(red) : instance(s) of non-positive definite covariance

Where X is

R : Radial detection (if other detection after, then lower case) :
I : In-track detection (if other detection after, then lower case)
C : Cross-track detection (if other detection after, then lower case)
X : Indeterminate (more than one particle "triggered" near same time)

The detection limit for directional versus isotropic seems to be about the same as before with a very high detection rate and near 100% detection for maneuvers greater than 1 m/s. Directional characterizations are most consistently found for the cross-track maneuvers. The radial maneuver particle causes most of the false maneuver detections (resulting in a lower-case letter in Table 3 versus an upper-case letter). In initial testing, with lower process noise values for the radial maneuver particle, false maneuver detections occur before the actual maneuver in many instances due to the radial particle. This is due to the phenomenon that changes in the radial direction are much less observable than the other two directions. The directional detection rate as a function of delta-V magnitude is shown in Figure 13 for the cases shown in Table 3. The directional characterization varies depending on thrust direction, achieving 100% accuracy over smaller delta-V magnitudes and falling off at higher magnitudes for cross-track maneuvers, 100% accuracy for mid-range delta-V magnitudes and falling off at both lower and higher magnitudes for radial maneuvers,

and about 50% accuracy for all delta-V magnitudes for in-track maneuvers. Incorrect classifications occur primarily with an "indeterminate" classification (where more than one particle "triggers" near the same time) as opposed to a classification in the wrong direction.

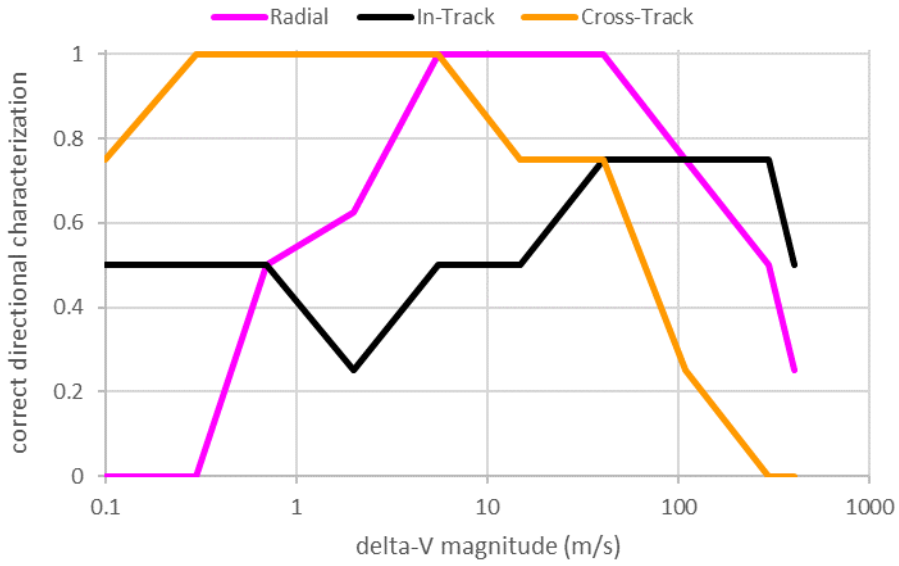

Figure 13. Fraction with correct direction characterization as function of delta-V magnitude showing different delta-V magnitude behavior based on maneuver direction.

5. SUMMARY

This paper focuses on the tracking of objects in cislunar orbits using an estimation filter and subsequent maneuver detection. We demonstrate that impulsive maneuvers can be detected and characterized using an IMM of varying process noise models with a near 100% accuracy. While this paper uses passive RF observations as the measurements, other observations or combinations of observations could be used instead. Note that large maneuvers, or maneuver particle process noise cases for these cislunar orbits in the vicinity of the Moon, can lead to problems within the estimation filter when UKF sigma point orbits pass too close to the Moon's center resulting in unrealistic object states.

Future research include (1) examining intermediate impulsive thrust directions, where more than one directional maneuver particle is relevant, (2) examining different cislunar periodic families where the detection/observability behavior vary from the exemplar orbit used in this paper, and (3) developing a different type of IMM using varying acceleration models to attempt to detect and characterize low-thrust maneuvers in cislunar orbits that take place over hours or even days.

6. REFERENCES

[1] C. Chow, C. Wetterer, K. Hill, C. Gilbert, D. Buehler and J. Frith, "Cislunar Periodic Orbit Families and Expected Observational Features.," in *The Advanced Maui Optical and Space Surveillance Technologies (AMOS) Conference, Maui, HI, September 15-18*, 2020.

[2] C. Chow, C. Wetterer, J. Baldwin, M. Dilley, K. Hill, P. Billings and J. Frith, "Cislunar Orbit Determination Behavior: Processing Observations of Periodic Orbits with Gaussian Mixture Model Estimation Filters," in The Advanced Maui Optical and Space Surveillance Technologies (AMOS) Conference, Maui, HI, September 14-17, 2021.

[3] Y. Bar-Shalom, P. K. Willett and X. Tian, Tracking and data fusion., Storrs, CT, USA: YBS publishing, 2011.

[4] GMAT Development Team, "User's Guide," 2020.